

## Article

# Astragalin Exerted Hypoglycemic Effect by Both Inhibiting $\alpha$ -Glucosidase and Modulating AMPK Signaling Pathway

Qian Li <sup>1,2,†</sup> , Zhangchang Yang <sup>1,3,†</sup>, Huijie Lu <sup>4</sup>, Fan Liu <sup>1</sup>, Donglai Zhou <sup>1</sup>  and Yuxiao Zou <sup>1,2,3,\*</sup> 

<sup>1</sup> Sericultural & Agri-Food Research Institute, Guangdong Academy of Agricultural Sciences, Key Laboratory of Functional Foods, Ministry of Agriculture and Rural Affairs, Guangdong Key Laboratory of Agricultural Products Processing, Guangzhou 510610, China; liq@gdaas.cn (Q.L.); yzx140484@163.com (Z.Y.); liufan@gdaas.cn (F.L.); zhoudonglai.2007@163.com (D.Z.)

<sup>2</sup> Guangdong Laboratory for Lingnan Modern Agriculture, Maoming 525000, China

<sup>3</sup> College of Food Science, South China Agricultural University, Guangzhou 510642, China

<sup>4</sup> Institute of Animal Science, Guangdong Academy of Agricultural Sciences, Guangzhou 510640, China; luhuijie@mail2.sysu.edu.cn

\* Correspondence: yuxiao\_zou@163.com; Tel.: +86-136-6892-7180; Fax: +86-20-87236354

† These authors contributed equal to this work.

**Abstract:** Background: The hypoglycemic activity of mulberry leaf polyphenols has been widely studied, while its mechanism of action needs further elucidation. Methods: The inhibitory activity mechanism of astragalin on  $\alpha$ -glucosidase was investigated with a combination of multispectroscopic techniques and molecular docking. The hypoglycemic pathway was further revealed with a high-glucose human hepatocellular carcinomas (HepG2) cell model. Results: The results indicated that astragalin inhibited  $\alpha$ -glucosidase with IC<sub>50</sub> of 154.5  $\mu$ M, which was the highest in potency among the main polyphenols from mulberry leaves. Astragalin could bind to  $\alpha$ -glucosidase with a single inhibition site and quench its endofluorescence with a static quenching mechanism. Astragalin changed the secondary structure of  $\alpha$ -glucosidase, and the decreased  $\alpha$ -helix content, representing the un-folding conformation, resulted in the decreased activity. The molecular docking further indicated that two sustainable hydrogen bonds were generated between astragalin and  $\alpha$ -glucosidase residue Ser-88 and Tyr-133. The main driving forces to form the astragalin- $\alpha$ -glucosidase complex were the van der Waals force and hydrogen bond. Astragalin at a concentration of 80  $\mu$ g/mL obtained the best hypoglycemic effect by activating the Adenosine 5'-monophosphate (AMP)-activated protein kinase (AMPK) signaling pathway. Conclusions: This study provides new insights into the potential utilization of astragalin-rich foods in the improvement of diabetes mellitus.



check for updates

Academic Editor: Lindsay Brown

Received: 23 December 2024

Revised: 21 January 2025

Accepted: 21 January 2025

Published: 23 January 2025

**Citation:** Li, Q.; Yang, Z.; Lu, H.; Liu, F.; Zhou, D.; Zou, Y. Astragalin Exerted Hypoglycemic Effect by Both Inhibiting  $\alpha$ -Glucosidase and Modulating AMPK Signaling Pathway. *Nutrients* **2025**, *17*, 406. <https://doi.org/10.3390/nu17030406>

**Copyright:** © 2025 by the authors. Licensee MDPI, Basel, Switzerland. This article is an open access article distributed under the terms and conditions of the Creative Commons Attribution (CC BY) license (<https://creativecommons.org/licenses/by/4.0/>).

**Keywords:** astragalin;  $\alpha$ -glucosidase; inhibitory mechanism; molecular docking; AMPK pathway

## 1. Introduction

Human physical and mental health has been seriously affected by metabolic diseases caused by modern lifestyle changes. At present, diabetes, together with cardiovascular diseases and cancer, has become one of the major chronic non-hereditary diseases threatening human health [1,2]. Glucose metabolism disorder is the main pathological feature for diabetes, and continuous hyperglycemia will cause cardiovascular and neurological complications. The mulberry leaf is a classic food material used in traditional Chinese medicine to treat diabetes, which has a long-term practical basis in folk health care and

clinical practice [3]. Modern scientific experiments also confirmed that flavonoids, polysaccharides, and polyhydroxyalkaloids in mulberry leaves were important material bases for its hypoglycemic effect [4,5].

Astragalins (kaempferol-3-O- $\beta$ -D-glucopyranoside) are active natural flavonoid ingredients extracted from various traditional medicine plants, such as *Morus alba* L. [4], *Moringa oleifera* L. [6], *Astragalus hamosus* [7], and *Eucommia ulmoides* L. [8]. They obtain various biological activities such as antioxidant [9], anti-inflammatory [10], and hypnotic effects [11]. Astragalins improve airway thickening and alveolar destruction by blocking airway allergic inflammation, thereby antagonizing asthma [11]. As one of the main flavonoids from *Morus alba* (both leaves and fruit), astragalins increased endogenous estrogen and progesterone in aged female rats [12]. However, whether astragalins play a role in the hypoglycemic effect of mulberry leaves needs further exploration.

The inhibitors inhibited the activity of  $\alpha$ -glucosidase in the small intestine and slowed down the breakdown of polysaccharides into monosaccharides and the subsequent absorption, resulting in reduced insulin secretion in pancreatic tissue and alleviated insulin resistance [13]. Currently, the  $\alpha$ -glucosidase inhibitors commonly applied in the adjuvant treatment for type-2 diabetes include miglitol, voglibose, and acarbose [1]. However, serious side effects were accompanied by the long-term use of these drugs [14]. Fortunately, dietary supplementation of natural active products with  $\alpha$ -glucosidase inhibitory activity, reducing or eliminating adverse secondary side effects, has been proven to be an effective method in controlling hyperglycemia.

Adenosine 5'-monophosphate (AMP)-activated protein kinase (AMPK, EC 2.7.11.31), a heterotrimeric protein composed of three subunits: alpha (63 kD), beta (30 kD), and gamma (37–63 kD) and belonging to serine/threonine protein kinase, plays a positive role in multiple signaling pathways regulating glucose metabolism homeostasis [15]. AMPK is mainly regulated by changes in the adenosine monophosphate/triphosphate (AMP/ATP) ratio and creatine/phosphocreatine ratio in cells [16]. Under the condition of hypoxia, glucose deficiency, and muscle activity, cells suffer from stress response characterized by ATP depletion, leading to the increase in the AMP/ATP ratio and the activation of AMPK [17]. AMPK activation stimulates the glucose uptake in muscle, fat, liver, pancreas and other organs, and inhibits endogenous glucose production, which plays an active role in preventing diabetes and improving metabolic syndrome [18].

The present study further compared the  $\alpha$ -glucosidase inhibitory activity of the main phenolic compounds in mulberry leaves. In addition, the most active compound, astragalins, was selected for the inhibitory mechanism analysis. Furthermore, a high-glucose HepG2 cell model was established to reveal the pathway through which astragalins regulated glucose homeostasis. To the best of our knowledge, no study has reported the inhibition mechanism of astragalins against  $\alpha$ -glucosidase. The results of this research will enrich the theoretical system of the substance basis for mulberry leaves' hypoglycemic effect.

## 2. Materials and Methods

### 2.1. Materials

Acarbose,  $\alpha$ -glucosidase, and p-nitrophenyl- $\alpha$ -D-glucopyranose (p-NPG) were purchased from Yuanye Biotechnology Co., Ltd., Shanghai, China. Standards such as astragalins, rutin, hyperoside, quercetin, gallic acid, gentic acid, chlorogenic acid, vanillic acid, caffeic acid, syringic acid, epicatechin, catechin, and benzoic acid were purchased from Qiyun Biotechnology Co., Ltd., Guangzhou, China, with a purity of >98%. HepG2 cells were purchased from Yuchi Biotechnology Co., Ltd., Shanghai, China. High-glucose Dulbecco's modified Eagle medium (DMEM), fetal bovine serum (FBS), nonessential amino acid (NEAA), trypsin, penicillin streptomycin dual antibody solution, phosphate buffer solu-

tion (PBS), and HBSS buffer solution were purchased from MIKX Biotechnology Co., Ltd., Shenzheng, China. Glucose, Total cholesterol (TC), and total triglyceride (TG) kits were purchased from Jiancheng Bioengineering Research Institute, Nanjing, China. The other reagents were all analytical grade with a purity of >99.8%.

## 2.2. $\alpha$ -Glucosidase Inhibitory Activity

The inhibition activity was carried out with the help of the substrate p-NPG, based on a previous study with slight modifications [19].  $\alpha$ -glucosidase solution (1 U/mL) was prepared with 0.1 mol/L PBS 50  $\mu$ L, together with astragaloside (112, 224, 336, 448, and 560  $\mu$ M) or acarbose (0.64, 1.28, 1.92, 2.56, and 3.2 mM) in a series of dilution concentrations, 50  $\mu$ L, were added to a 96-well plate and incubated at 37 °C for 10 min. Then, 50  $\mu$ L of 2 mmol/L p-NPG was added continually and incubated at 37 °C for another 20 min. Further, the enzyme activity was reduced by placing the well plate in an ice water bath for 5 min. Finally, 50  $\mu$ L of 1 mol/L  $\text{Na}_2\text{CO}_3$  was added to terminate the reaction, and the absorbance values were measured at 405 nm. The inhibition rates of  $\alpha$ -glucosidase were calculated according to Formula (1), and the half maximal inhibitory concentrations ( $\text{IC}_{50}$ ) were obtained by nonlinear regression fitting.

$$\text{Enzyme activity inhibition rate (\%)} = [1 - (A_a - A_b)/(A_c - A_d)] 100\% \quad (1)$$

$A_a$ : sample group absorbance;  $A_b$ : sample background absorbance (equal volume buffer instead of enzyme solution);  $A_c$ : control group absorbance (equal volume buffer instead of sample solution); and  $A_d$ : control background absorbance (equal volume buffer instead of sample and enzyme solution).

## 2.3. Multi-Fluorescence Spectroscopy

Astragaloside in different concentrations (0, 10, 20, 50, 80, 100, 120, and 150  $\mu$ g/L) were mixed with  $\alpha$ -glucosidase (1 U/mL), and incubated for 5 min at three temperatures (298 K, 304 K, and 310 K). The mixture was scanned using fluorescence spectroscopy (SpectraMax i3x, Molecular Devices, LLC., San Jose, CA, USA). The excitation wavelength was set at 280 nm, and the emission wavelength at 300–500 nm, with excitation and emission slit widths of 5 nm. Then, the following Stern–Volmer dynamic collision quenching equations were applied to calculate the fluorescence quenching parameters, including the quenching constants ( $K_{SV}$ ), quenching rate constant ( $K_q$ ), binding constant ( $K_a$ ), and binding site number ( $n$ ) [20]. The equations are described below [1]:

$$\frac{F_0}{F} = 1 + K_{SV}[Q] = 1 + K_q\tau_0[Q] \quad (2)$$

$$\lg \frac{F_0 - F}{F} = \lg K_a + n \lg [Q] \quad (3)$$

$F$  and  $F_0$  were the peak fluorescence intensities for  $\alpha$ -glucosidase with and without astragaloside, respectively;  $[Q]$  was the astragaloside concentration; and  $T_0$  was the average lifespan of the protein ( $10^{-8}$  s).

## 2.4. FT-IR Measurements

The secondary conformation of  $\alpha$ -glucosidase (1 U/mL) with or without sample treatment were detected with a Fourier transform infrared spectrometer (FT-IR) (VERTEX 7.0, BRUKER Co., Ltd., Bremen, Germany), by fitting the infrared amide type I curve ( $1600\text{--}1700 \text{ cm}^{-1}$ ) [21]. The final concentration of astragaloside was 100  $\mu$ g/mL.

## 2.5. Molecular Docking

### 2.5.1. Visual Docking

The molecular docking was performed with AutoDock Vina 1.1.2 software (Scripps Research Institute, Olson Lab, San Diego, CA, USA) [22]. The crystal structure of the  $\alpha$ -glucosidase protein was retrieved from the PDB database (PDB id: 5NN4). The 3D structure of astragaloside was downloaded from the pubchem database, and MMFF94 force field was applied for energy minimization.

The  $\alpha$ -glucosidase protein (EC 3.2.1.20) was processed with PyMol 2.5.2 prior to docking, and the docking box was set as Pymol plugin center\_of mass.py. The ADFRsuite 1.0 (Scripps Research Institute, Olson Lab, San Diego, CA, USA) was used to convert into the PDBQT format required for AutoDock Vina 1.1.2 docking. The conformation with the highest output score was considered as the binding conformation, and PyMol 2.5.2 was used for the consequent visual analysis.

### 2.5.2. Molecule Dynamics Simulation

Based on the conformation molecular docking as the initial structure, the full atom molecular dynamics simulation was carried out using AMBER 18 software (Scripps Research Institute, Olson Lab, San Diego, CA, USA) [23]. The antechamber module and the Hartree-Fock (HF) SCF/6-31G\* of Gaussian 09 software were combined to calculate the charge of small molecules (Scripps Research Institute, Olson Lab, San Diego, CA, USA). In addition, the 2500-step steepest descent method and 2500-step conjugate gradient method were applied to optimize the energy of the system. The particle mesh Ewald (PME) method was employed to calculate electrostatic interactions, the SHAKE method was used to limit hydrogen atom bond lengths, and the Langevin algorithm was applied for temperature control. The collision frequency  $\gamma$ , the system pressure, and the integration step size was set to  $2 \text{ ps}^{-1}$ , 1 atm, and 2 fs, respectively, and the trajectory was saved every 10 ps for subsequent analysis.

### 2.5.3. MMGBSA Binding Free Energy

The molecular mechanics generalized born surface area (MM/GBSA) method was applied to calculate the binding free energy. A 90–100 ns MD trajectory was used for the calculation with the formula shown below [24]:

$$\begin{aligned} \Delta G_{\text{bind}} &= \Delta G_{\text{complex}} - (\Delta G_{\text{receptor}} + \Delta G_{\text{ligand}}) \\ &= \Delta E_{\text{internal}} + \Delta E_{\text{VDW}} + \Delta E_{\text{elec}} + \Delta G_{\text{GB}} + \Delta G_{\text{SA}} \end{aligned} \quad (4)$$

$\Delta E_{\text{internal}}$ : internal energy, including bond energy ( $E_{\text{bond}}$ ), angular energy ( $E_{\text{angle}}$ ), and torsional energy ( $E_{\text{torsion}}$ ),  $\Delta E_{\text{VDW}}$ : van der Waals interaction, and  $\Delta E_{\text{elec}}$ : electrostatic interaction.  $\Delta G_{\text{GB}}$ : polar solvation free energy;  $\Delta G_{\text{SA}}$ : non-polar solvation free energy.

## 2.6. Cell Experiment

### 2.6.1. HepG2 Cell Culture

HepG2 cells at 10 to 40 generations were configured at a concentration of  $4 \times 10^5$  /mL. The cells suspension 100  $\mu\text{L}$  was inoculated into a culture plate with DMEM (10 mL) containing glucose 4.5 g/L, 10% FBS, penicillin (1000 U/mL), and streptomycin (10 mg/mL), and cultivated in a 37 °C, 5% CO<sub>2</sub> incubator.

### 2.6.2. HepG2 Cell Survival Rate

Astragaloside (30, 50, 80, 100, and 200  $\mu\text{g}/\text{mL}$ ) was configured at different concentrations. Each sample was added to a 96-well plate with HepG2 cells and incubated in a 37 °C, 5%

CO<sub>2</sub> incubator for 24 h. After washing twice with PBS, the CCK-8 solution 100 µL was added, and incubated for another 4 h. The absorbance at 450 nm was measured using a Microplate reader (Bio TekGen5, BioTech Instruments, Co., Ltd., Winooski, VT, USA). The cells' survival rates were calculated based on the formula as shown below:

$$\text{Cell survival rate (\%)} = A \text{ samples} / A \text{ black control} \times 100\% \quad (5)$$

### 2.6.3. The Establishment of HepG2 High Glucose Model

When the cells were increased to about 80%, insulin at a concentration of 10<sup>-5</sup> mmol/L was treated for 24 h to induce the formation of insulin-resistant cells [25]. Six experimental groups were set for the comparison, namely, black (normal control without insulin treatment), model (insulin treatment control), acarbose (5 µg/mL positive control with insulin treatment), and astragalin sample groups (20, 80, and 200 µg/mL, with insulin treatment). After the treatment of 24 h with different samples, the glucose, TC, and TG content in the HepG2 cell supernatant was measured with glucose, TC, and TG assay kits.

### 2.6.4. Western Blotting

The proteins in the above six cell sample groups (black, model, acarbose, and astragalin 30, 80, and 200 µg/mL) were extracted with a total protein extraction buffer, and the concentration was detected with bicinchoninic acid (BCA) assay kits. Protein samples of 20 µg were separated by sodium dodecyl sulfate polyacrylamide gel electrophoresis in the Bio-Rad electrophoresis apparatus (Liuyi Biotechnology Co., Ltd., Beijing, China), and then transferred to polyvinylidene fluoride membranes. The electrophoretic proteins were sealed with 5% skimmed milk at room temperature for 1 h, and the membranes were incubated overnight with primary antibodies, including AMPK, phospho-AMPK (p-AMPK), acetyl CoA carboxylase (ACC, EC 6.4.1.2), and glucose transporter 4 (GLUT4) at 4 °C. After washing the membrane with phosphate-buffered saline tween-20, the membranes were incubated with secondary antibodies at room temperature for 1 h.

### 2.7. Statistical Analysis

The experiments were carried out in triplicate. The data analysis and figure drawing were processed with a combination of SPSS 22, Microsoft Excel 2010, Origin 8.0, and GraphPad Prism 9 software. The differences were considered significant when  $p < 0.05$ , and examined through a one-way analysis of variance (ANOVA).

## 3. Results and Discussion

### 3.1. The $\alpha$ -Glucosidase Inhibitory Effect of the Main Polyphenols in Mulberry Leaves

The main polyphenols in mulberry leaves included astragalin, rutin, chlorogenic acid, benzoic acid, epicatechin, catechin, vanillic acid, etc., which had been reported by our previous research [4]. The results of the present study comparing their  $\alpha$ -glucosidase inhibition indicated that the activity of astragalin was the highest, with an IC<sub>50</sub> value of 154.5 µM (Figure 1A), while the IC<sub>50</sub> values of the other main polyphenols from mulberry leaves were all greater than 500 µM. Although the activity of astragalin was weak compared to acarbose (1.35 µM) (Figure 1B), it obtained a wide range of plant sources and safety. The activity of astragalin was superior to that of the reported compounds rutin, isoquercetin [26], 2,4-dimethoxy-6,7-dihydroxyphenanthrene [27], phlorizin [1], and batatasin I [28], with IC<sub>50</sub> of 198 µM, 185 µM, 400 µM, 0.98 mM, and 2.55 mM, respectively. In addition to astragalin, the alkaloids such as 1-Deoxynojirimycin and its derivatives in mulberry leaves exhibited a strong  $\alpha$ -glucosidase inhibitory activity, thereby exerting a hypoglycemic activity [5]. The hypoglycemic effects of astragalin were verified in streptozocin-induced diabetic mice, which improved the glucose tolerance and reduced the level of glucose [29]. In addition,

astragalin decreased the over-expression of the vascular endothelial growth factor in Müller cells, and alleviated diabetic retinopathy caused by high glucose [30]. Meanwhile, the  $\alpha$ -glucosidase inhibition and hypoglycemic activity mechanism were indeed lacking.

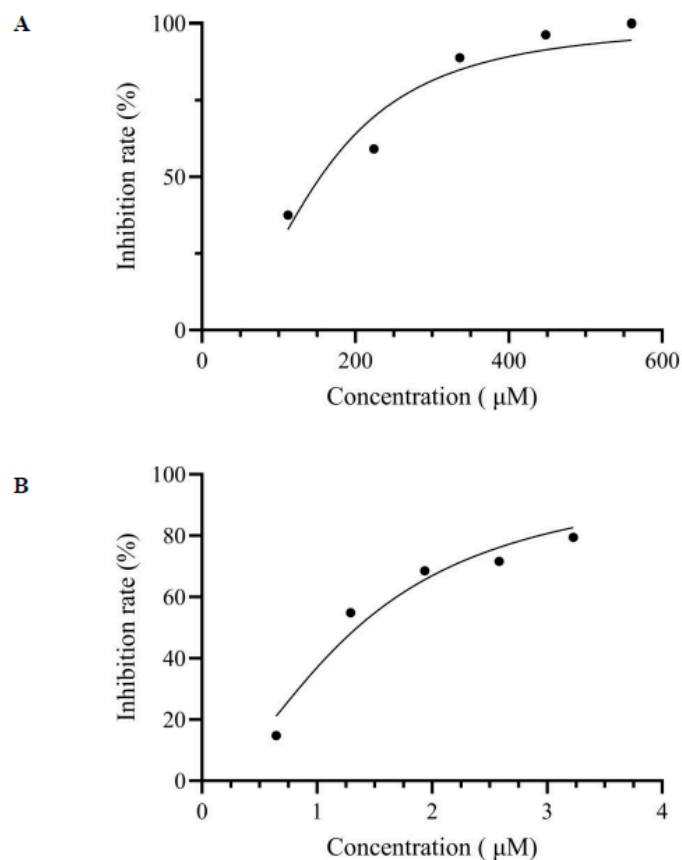


**Figure 1.** The inhibition rate for  $\alpha$ -glucosidase under different concentrations of inhibitor. (A) Astragalin; (B) acarbose.

### 3.2. Binding Mechanism and Properties by Fluorescence Spectroscopy

Dynamic quenching is formed by the collision between quencher and molecules-excited fluorescence, while static quenching is the formation of a complex through binding [31]. Proteins containing aromatic amino acids, such as tryptophan (try), tyrosine (tyr), and phenylalanine (phe), emit fluorescence at an excitation wavelength of 280 nm, while the intrinsic fluorescence intensity decreased when interacting with quenchers [32]. The free  $\alpha$ -glucosidase had a maximum fluorescence emission peak around 346 nm, the fluorescence intensity decreased dose-dependently with the increase in astragaline concentration, and the maximum emission wavelength increased to 349 nm (Figure 2A). This red-shift phenomenon was caused by the unfolding of the  $\alpha$ -glucosidase structure during the interaction with astragaline, exposing the fluorescent residues (try, tyr, and phe) to a more hydrophilic environment [33]. The results are consistent with previous studies [1,19], and astragaline induced microenvironment changes in the fluorophore of  $\alpha$ -glucosidase.

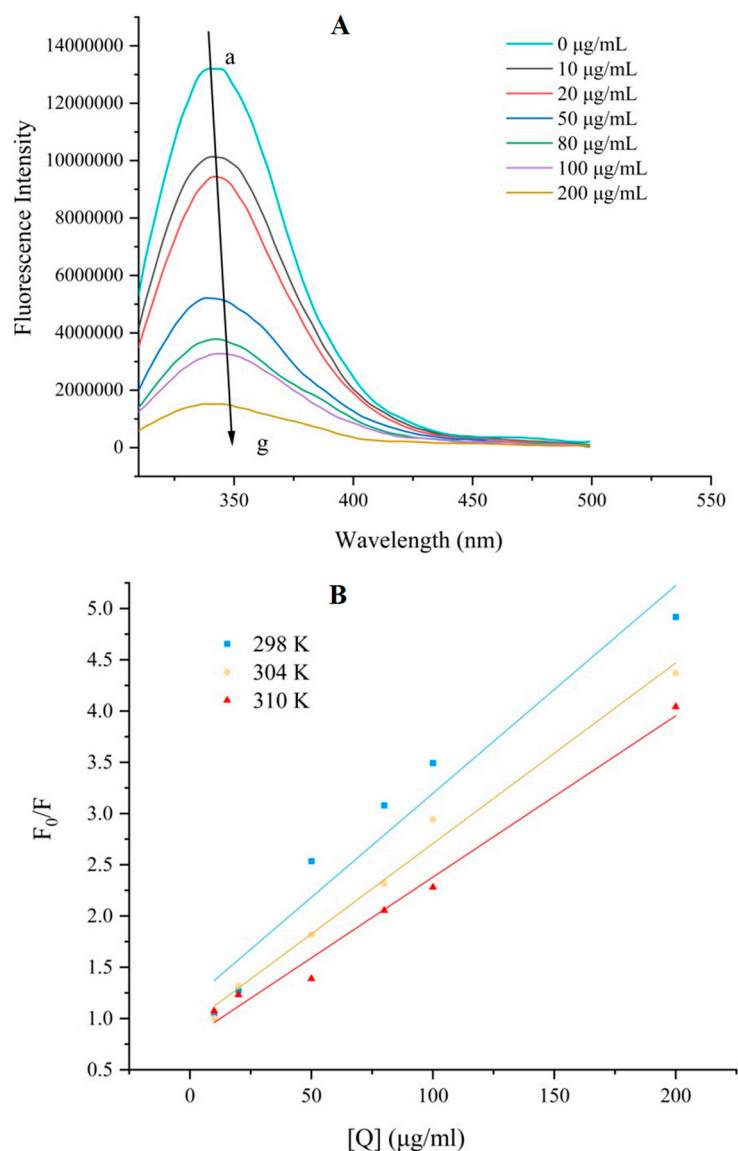


**Figure 2.** Fluorescence spectra of  $\alpha$ -glucosidase with astragaline. (A) Fluorescence curves at 298 K in the present of increasing concentrations, (B) Stern–Volmer plots at different temperatures. Note: a–g represented the concentration of 0–200  $\mu\text{g}/\text{mL}$ .

The Stern–Volmer curves of astragaline with  $\alpha$ -glucosidase showed a good linear relationship (Figure 2B), and the  $K_{SV}$  value decreased with the increase in temperature (Table 1), indicating that the interaction between astragaline and  $\alpha$ -glucosidase was supposed to be static quenching. The maximum diffusion collision quenching constant of the quencher for biomolecules is  $2.0 \times 10^{10} \text{ Lmol}^{-1} \text{ s}^{-1}$ . Under three temperature conditions, the  $K_q$  values of astragaline with  $\alpha$ -glucosidase were much higher than  $2.0 \times 10^{10} \text{ Lmol}^{-1} \text{ s}^{-1}$ , proving the static quenching interaction mechanism and the formation of a complex with  $\alpha$ -glucosidase [1,34]. The number of binding sites ( $n$ ) for astragaline with  $\alpha$ -glucosidase were close to one under three different temperatures, indicating a 1:1 molar ratio of interaction and possessing one binding site. The  $K_a$  values of astragaline with  $\alpha$ -glucosidase decreased with the increase in temperature (298–310 K), indicating a reduction in the complex stability [22].

**Table 1.** The quenching constants ( $K_{SV}$ ), binding constants ( $K_a$ ), and binding site ( $n$ ) for the interaction of astragalín with  $\alpha$ -glucosidase.

T (K)	$K_{SV}$ ( $\times 10^3$ L mol $^{-1}$ )	R <sup>a</sup>	$K_q$ ( $\times 10^{11}$ L mol $^{-1}$ )	$K_a$ ( $\times 10^5$ L mol $^{-1}$ )	$n$	R <sup>b</sup>
298	9.093	0.97	9.093	4.29	1.238	0.98
304	7.903	0.99	7.903	3.01	1.1905	0.96
310	7.061	0.97	7.061	2.56	0.8446	0.96

Note: R<sup>a</sup> is the correlation coefficient for the  $K_{SV}$  values; R<sup>b</sup> is the correlation coefficient for the  $K_a$  values.

### 3.3. FT-IR Analysis

The protein secondary structure could be altered by binding with phenolic compounds [13]. The effect of astragalín on the  $\alpha$ -glucosidase structure was further investigated using FT-IR spectroscopy, which indicated that the binding of astragalín with  $\alpha$ -glucosidase changed the secondary structure of the protein, thereby affecting the enzyme activity. The amide I band (1600 cm $^{-1}$ –1700 cm $^{-1}$ , derived from the stretching vibration of  $-C=O$ ) is more sensitive to the protein secondary structural changes than the amide II band (1500 cm $^{-1}$ –1600 cm $^{-1}$ , mainly consisting of C-N stretching vibration and N-H bending vibration peaks) [35]. As shown in Figure 3A, the peak intensity was significantly enhanced in the astragalín/ $\alpha$ -glucosidase complex; the absorption peak at 1541.1 cm $^{-1}$  in the amide II band in  $\alpha$ -glucosidase was enhanced significantly with the treatment with astragalín.

The relative content of the amide I band in the protein secondary structure was determined using a curve-fitting protocol coupled with second-derivative resolution enhancement (Figure 3B,C). The results indicated that, with the addition of astragalín, the  $\alpha$ -helix,  $\beta$ -turn,  $\beta$ -sheet, and random coil of  $\alpha$ -glucosidase changed from 62.47%, 11.72%, 11.94%, and 21.08%, to 29.94%, 19.30%, 4.71%, and 38.79%. The  $\alpha$ -helix content of the  $\alpha$ -glucosidase secondary structure was significantly decreased from 62.47% (Figure 3B) to 29.94% (Figure 3C). The  $\alpha$ -helix around the catalytic site of the enzyme was confirmed to play a crucial role in stabilizing the activity. It was speculated that the decrease in the  $\alpha$ -helix content was related to the decrease in the  $\alpha$ -glucosidase activity [36]. The results confirmed that astragalín induced the partial unfolding of the  $\alpha$ -glucosidase conformation. The interaction between astragalín and the  $\alpha$ -glucosidase  $-C=O$  group subunits resulted in the rearrangement of the  $\alpha$ -glucosidase secondary structure, thereby reducing the  $\alpha$ -glucosidase activity [33,37].

### 3.4. Molecular Docking Results for Astragalín with $\alpha$ -Glucosidase

Molecular docking was employed to further explore the binding mechanism of active molecules to macromolecular proteins [38]. The negative binding affinity indicated the possibility of binding; usually, a value less than  $-6$  kcal/mol was considered to have a high binding probability. The binding affinity score for the astragalín/ $\alpha$ -glucosidase complex was  $-7.238$  kcal/mol based on molecular docking, indicating that astragalín had a good binding potential with  $\alpha$ -glucosidase. The  $\alpha$ -glucosidase active pocket was a hydrophobic cavity based on a previous report [39]. The visual binding complex formed by astragalín with  $\alpha$ -glucosidase is exhibited in Figure 4. Astragalín was bound to the internal active pocket of the  $\alpha$ -glucosidase protein (Figure 4A–C). The active pocket was constructed by the surrounding of Val-84, Pro-217, Pro-130, Pro-131, Val-236, Ala-237, Pro-238, Ser-88, Tyr-133, and Ser-325 amino acid. Among them, astragalín underwent hydrophobic interactions with Val-84, Pro-217, Pro-130, Pro-131, Val-236, Ala-237, and Pro-238 on the active binding site, while forming hydrogen bonding interactions with Ser-88 and Tyr-133. These interactions were supposed to be the main reason for the stable binding of the astragalín with  $\alpha$ -glucosidase [40]. This visual result further confirmed one binding site in the fluorescence spectroscopy.

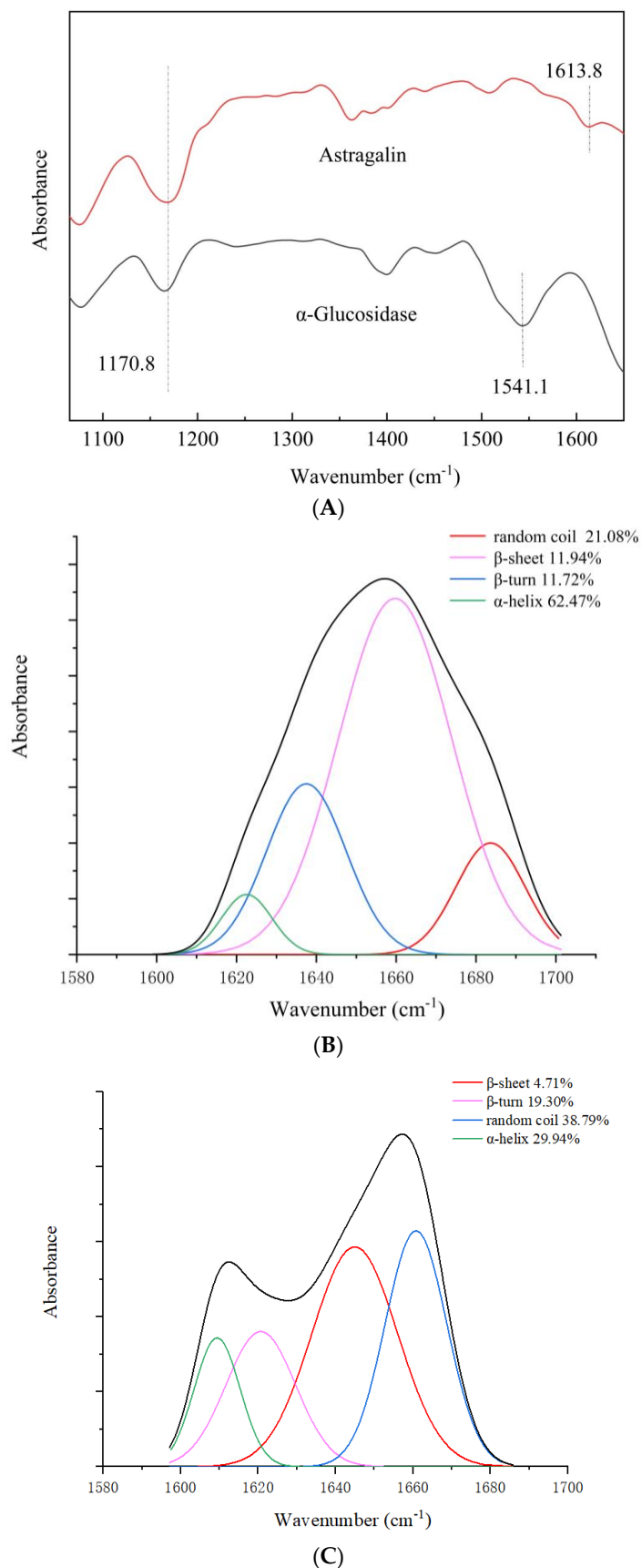


**Figure 3.** The FT-IR spectra of  $\alpha$ -glucosidase with astragalalin. (A) FT-IR curves, (C)  $\alpha$ -glucosidase in the absence of astragalalin (1 U/mL), and (B)  $\alpha$ -glucosidase with astragalalin (100  $\mu\text{g/mL}$ ). Note: the black line represented the overall secondary structure total fluorescence structure with a value of 100%.

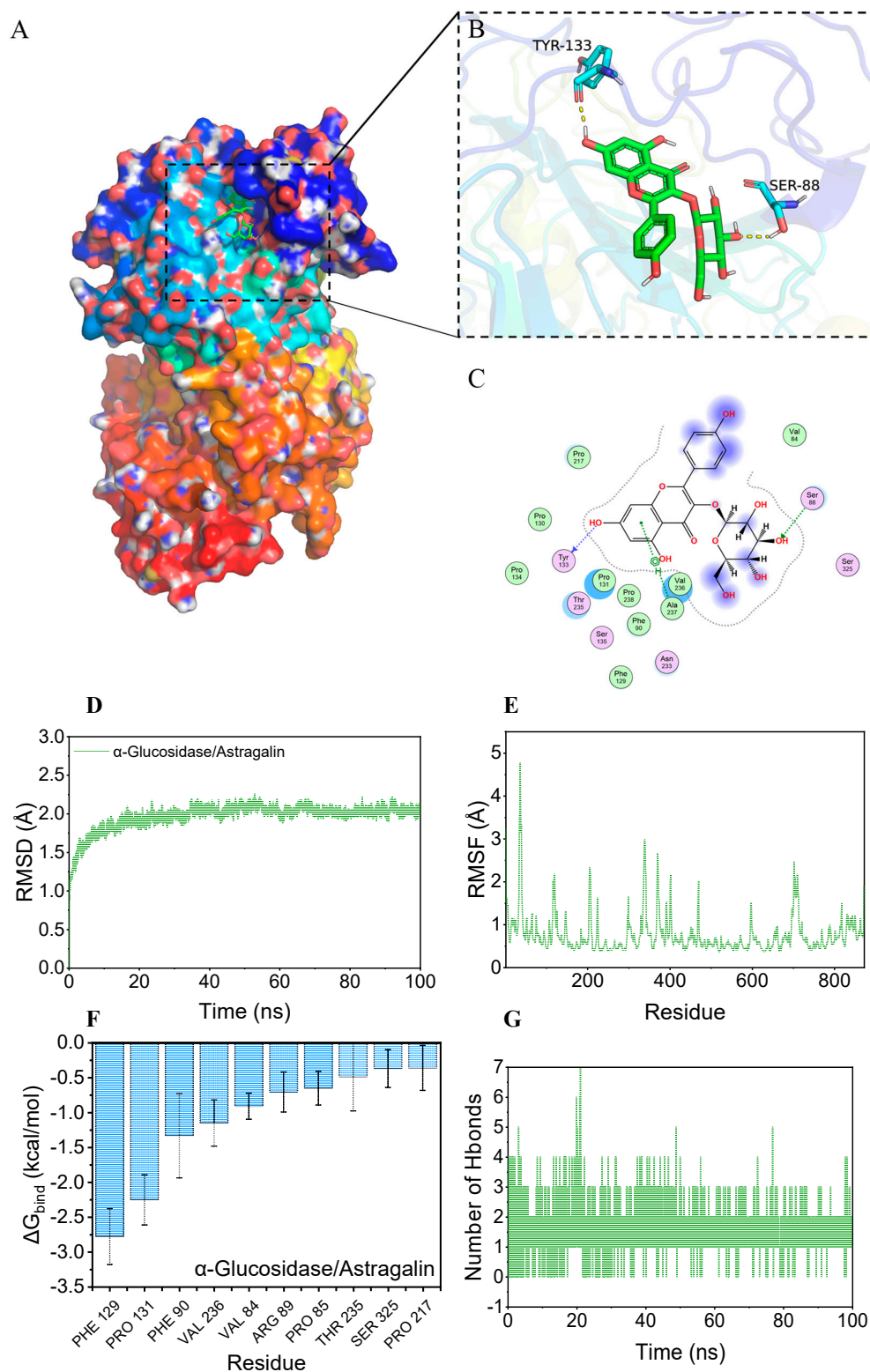


**Figure 4.** Binding diagram and dynamics simulation of  $\alpha$ -glucosidase with astragalol. (A) Overall view of 3D binding diagram, (B) partial view; astragalol is represented by the green stick, amino acid residues of the binding site are represented by light blue, and hydrogen bonding is represented by the yellow dashed line. (C) 2D interaction diagram. (D) Root mean square deviation (RMSD), and (E) root mean square fluctuation value (RMSF) based on molecular dynamics simulation. (F) Top 10 amino acid residues contributing to the binding of  $\alpha$ -glucosidase with astragalol. (G) The number of hydrogen bonds between astragalol and  $\alpha$ -glucosidase changes during the molecular dynamics simulation.

During the molecular dynamics simulation, a high root mean square deviation (RMSD) represented intense fluctuation and motion for the docking complex [41]. As shown in Figure 4D, there was no significant RMSD change for the astragaline/ $\alpha$ -glucosidase complex, indicating the high stability of the complex and the correction of the simulation parameters. The root mean square fluctuation (RMSF) reflected the flexibility of the protein [36]. The flexibility decreased when the protein combined with active molecules, thereby achieving complex stabilization and activity inhibition. As shown in Figure 4F, except for a small part of the  $\alpha$ -glucosidase protein, the RMSF of the complex was sustained within 2 angstroms, indicating that the main protein complex structure obtained a very high rigidity, which might be achieved by the combination with astragaline.

Based on the trajectory of the dynamics simulation, the binding energy was calculated using the MM-GBSA method, which more accurately reflected the binding effect between molecules and target proteins [22]. The binding energy ( $\Delta G_{\text{bind}}$ ) of astragaline/ $\alpha$ -glucosidase was  $-21.95 \pm 1.21$  kcal/mol (Table 2), indicating a strong binding affinity. The main contributions to the binding were the van der Waals energy and electrostatic energy. The top 10 amino acids that contribute to the binding, namely Phe-129, Pro-131, Phe-90, Val-236, Val-84, Arg-89, Pro-85, Thr-235, Ser-325, and Pro-217, respectively, which were the key amino acids, and the corresponding residue energy are exhibited in Figure 4F. The hydrogen bonds number between astragaline and  $\alpha$ -glucosidase was monitored during a 100 ns dynamics simulation, which was the strongest noncovalent interaction. The number of hydrogen bonds ranged from 0 to 7, most of the time being concentrated at 2, indicating that hydrogen bonding contributed to the stable binding of astragaline and  $\alpha$ -glucosidase [38].

**Table 2.** Binding free energies and components predicted by MM/GBSA (kcal/mol).

System Name	Alpha-Glucosidase/Astragaline
$\Delta E_{\text{vdw}}$	$-29.99 \pm 2.64$
$\Delta E_{\text{elec}}$	$-23.18 \pm 2.81$
$\Delta G_{\text{GB}}$	$35.65 \pm 2.66$
$\Delta G_{\text{SA}}$	$-4.43 \pm 0.44$
$\Delta G_{\text{bind}}$	$-21.95 \pm 1.21$

$\Delta E_{\text{vdw}}$ : van der Waals energy;  $\Delta E_{\text{elec}}$ : electrostatic energy;  $\Delta G_{\text{GB}}$ : electrostatic contribution to solvation;  $\Delta G_{\text{SA}}$ : non-polar contribution to solvation; and  $\Delta G_{\text{bind}}$ : binding free energy.

### 3.5. HepG2 Cell Experiments

The liver is one of the important sites for glucose metabolism; the regulatory mechanisms of glucose metabolism were extensively studied by many researchers, based on liver cell models [25,42]. The CCK-8 results for astragaline indicated that concentrations from 0–200  $\mu\text{g/mL}$  were within the safe range on HepG2 cells (Figure 5A). The high glucose model was induced successfully by insulin in HepG2 cells, where the glucose level was increased significantly from 3.43 mmol/L (Black) to 11.28 mmol/L (Model). In the model group, insulin resistance was induced, leading to the decrease in the glucose consumption and the large accumulation of glucose in the cells [25]. At concentrations of 20, 80, and 200  $\mu\text{g/mL}$ , astragaline reduced the glucose level in the cells, and the activity was the strongest at a concentration of 80  $\mu\text{g/mL}$ , which was superior to that of acarbose as positive control drug (5  $\mu\text{g/mL}$ ) (Figure 5B). In addition, the content of TC and TG also significantly increased in the model group, and astragaline under different concentrations reduced the levels of TC and TG in high-glucose HepG2 cells (Figure 5C,D).

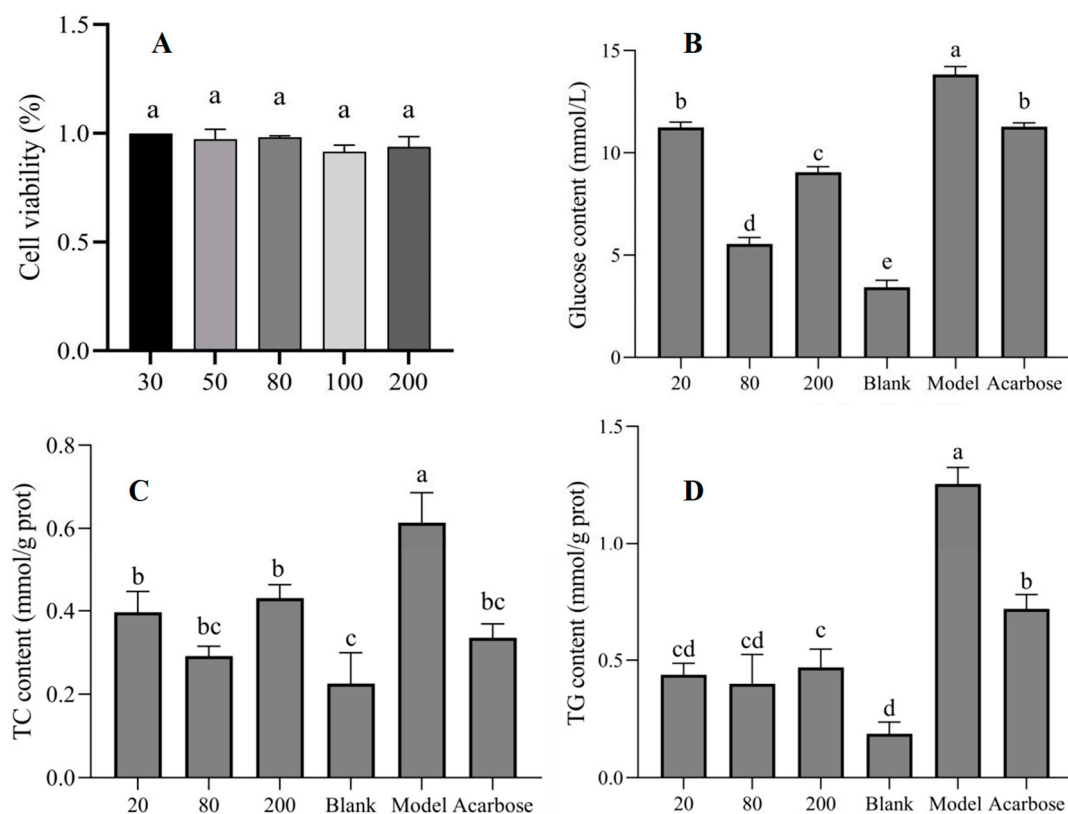


**Figure 5.** Effect of astragalgin on glucose homeostasis regulation. (A) CCK-8 under different treatment concentrations ( $\mu\text{g}/\text{mL}$ ), (B) intracellular glucose level, (C) intracellular TC level, and (D) intracellular TG level. Note: groups with different characters (a, b, c, d, and e) represented significant differences.

The results from the Western blotting (Figure 6) show that astragalgin under concentrations of 80 and 200  $\mu\text{g}/\text{mL}$  up-regulated the protein expression level of p-AMPK protein in high-glucose HepG2 cells with the activation of the AMPK pathway (Figure 6A,B). The activity of the rate-limiting enzyme in liver glucose metabolism was closely related to the activation of the AMPK pathway, which stimulated the phosphorylation of phosphofructose-2-kinase to promote glycolysis, and reduced the expression of fructose-1,6-diphosphatase to inhibit gluconeogenesis [43]. In addition, the acetyl CoA carboxylase (ACC) protein expression level was significantly down-regulated in the 80  $\mu\text{g}/\text{mL}$  concentration group (Figure 6C), which might contribute to the highest hypoglycemia activity in this group. The increase in ACC expression promoted fat synthesis by producing malonyl-CoA, which is utilized by fatty acid synthase to produce palmitic acid [3]. In addition, the protein expression level of glucose transporter 4 (GLUT4) significantly increased in the 20  $\mu\text{g}/\text{mL}$  group (Figure 6D), indicating a significant increase in glucose transport levels, thereby enhancing glucose consumption and glycogen synthesis [25,44]. The action pathway for astragalgin was similar to that of the previously reported phenolic compounds. Resveratrol activated the downstream ACC through AMPK, thereby improving the glucose level and inhibiting liver fat accumulation [45]. *p*-coumaric acid promoted the p-AMPK protein expression level in L6 skeletal muscle cells and increased ACC phosphorylation, thereby reducing glucose levels and promoting the  $\beta$ -oxidation of fatty acids [46]. In addition to polyphenols, recent studies have found that many compounds could activate the AMPK signaling pathway. Glutamine prevented intervertebral disc degeneration by decreasing AMPK lactylation and inhibiting glycolysis [47]. Fingolimod inhibited apoptosis in type 2 diabetic mice via activating the AMPK/mammalian target of the rapamycin (mTOR) signaling pathway [48].

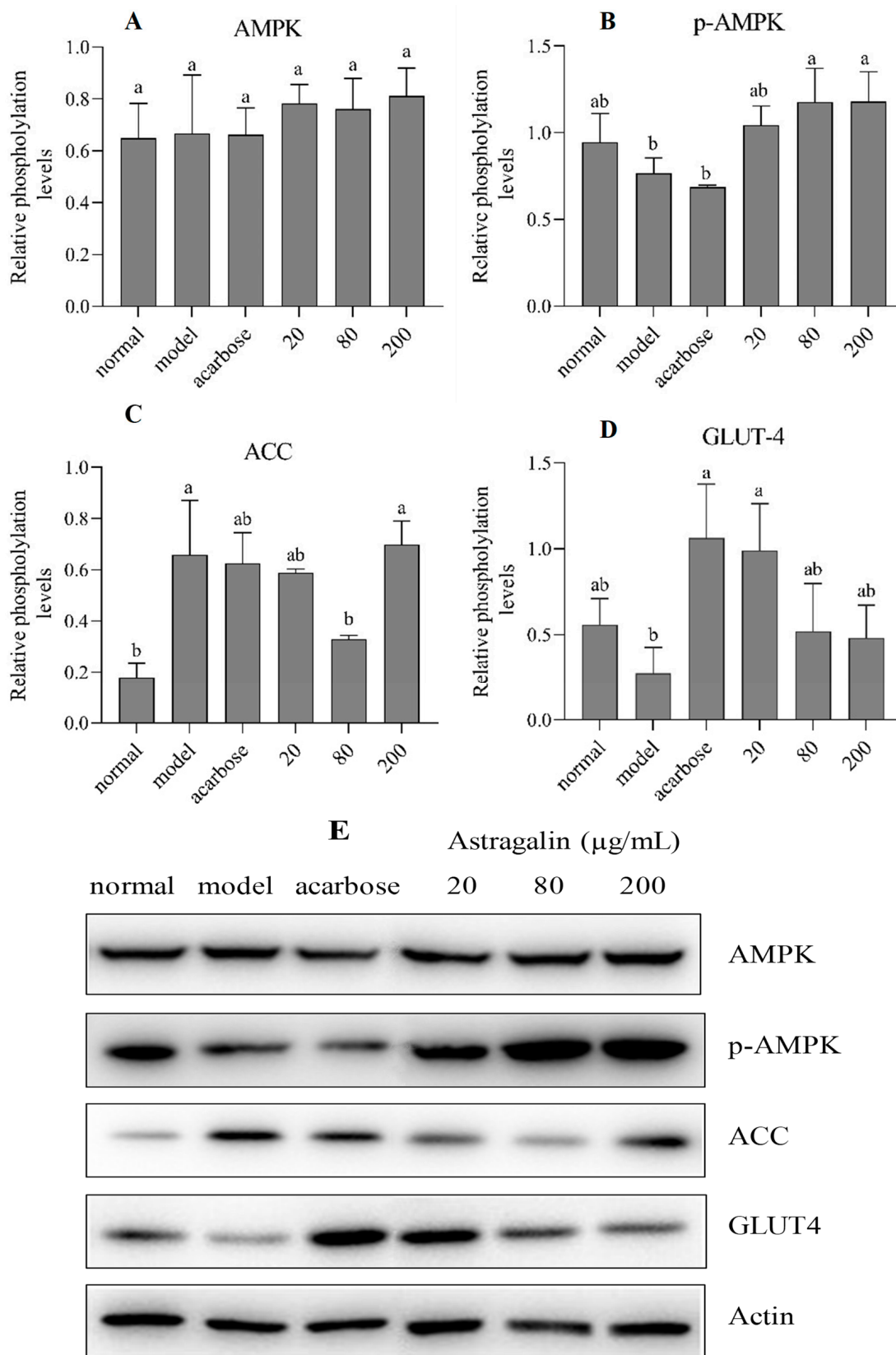


**Figure 6.** Expression level of the proteins related to glucose (A) AMPK, (B) p-AMPK, (C) ACC, (D) GLUT4, and (E) Grayscale image for the Western blot. Note: groups with different characters (a or b) represented significant differences.

## 4. Conclusions

Overall, astragalin obtained a potential hyperglycemic activity as evidenced by the  $\alpha$ -glucosidase inhibition activity and the reduction in the glucose level in HepG2 cells. The results indicated that astragalin was an effective  $\alpha$ -glucosidase inhibitor with the  $IC_{50}$  of 154.5  $\mu$ M, which was the lowest concentration among the main polyphenols from mulberry leaves. The intrinsic fluorescence of  $\alpha$ -glucosidase was quenched by the interactions with astragalin in a single inhibition site through a static quenching mechanism. Meanwhile, the interactions changed the micro-environments and conformation of  $\alpha$ -glucosidase, and the decrease in  $\alpha$ -helix content, representing the secondary structure un-folding conformation, resulted in the decreased activity. The exact binding site of astragalin on  $\alpha$ -glucosidase was displayed by molecular docking. Astragalin at a concentration of 80  $\mu$ g/mL obtained the best hypoglycemic effect on the high-glucose HepG2 cell model, which exerted effects by activating the AMPK signaling pathway. Our research further enriched the theoretical basis for the design of hypoglycemic functional foods with mulberry leaves. Currently, fresh vegetables, tea, and hypoglycemic functional health foods made from mulberry leaves have been widely recognized by consumers. However, further research and development are still needed for hypoglycemic products containing astragalin. In our opinion, research on the digestion, absorption, intestinal metabolism, and functional targets of astragalin will help promote the industrial application of plant/pure astragalin.

**Author Contributions:** Conceptualization, Q.L.; Formal analysis, Q.L., Z.Y., F.L. and D.Z.; Investigation, Q.L., Z.Y. and H.L.; Resources, Q.L. and Y.Z.; Data curation, Z.Y., H.L. and F.L.; Writing—original draft, Q.L.; Writing—review & editing, Q.L.; Supervision, Y.Z.; Project administration, Q.L. and Y.Z.; Funding acquisition, Q.L. and Y.Z. All authors have read and agreed to the published version of the manuscript.

**Funding:** This research received funding from the Collaborative Innovation Center of GDAAS [No. XT202502; No. XT202229], and the Science & Technology Projects of Guangdong Province [No. 2022A1515010930; No. 2024A1515011122; No. 2023B0202010004]. The authors would like to acknowledge the contribution of the China Agriculture Research System of MOF and MARA [No. CARS-18-ZJ0503] and Key Science & Technology Research Projects of Foshan City [No. 2220001018588].

**Institutional Review Board Statement:** Not applicable.

**Informed Consent Statement:** Not applicable.

**Data Availability Statement:** The original contributions presented in this study are included in the article. Further inquiries can be directed to the corresponding author.

**Conflicts of Interest:** The authors declare that they have no financial interests or personal relationships which influenced the work reported in this paper.

## References

1. Xu, Z.; Kseniya, H.; Kraskouski, A.; Yang, Y.; Huang, Z.; Zhao, Z. Inhibition of  $\alpha$ -glucosidase activity and intestinal glucose transport to assess the in vivo anti-hyperglycemic potential of dodecyl-acylated phlorizin and polydatin derivatives. *Food Funct.* **2024**, *15*, 4785–4804. [[CrossRef](#)] [[PubMed](#)]
2. Sun, H.; Saeedi, P.; Karuranga, S.; Pinkepank, M.; Ogurtsova, K.; Duncan, B.B.; Stein, C.; Basit, A.; Chan, J.C.N.; Mbanya, J.C. IDF Diabetes Atlas: Global, regional and country-level diabetes prevalence estimates for 2021 and projections for 2045. *Diabetes Res. Clin. Pract.* **2022**, *183*, 109119. [[CrossRef](#)]
3. Zou, Y.; Shi, Y.; Liu, F.; Li, E.; Yang, Q.; Chen, R.; Li, Q. The synergistic lipogenesis inhibition and molecular mechanism of polyphenols and polysaccharides from mulberry leaf. *Food Biosci.* **2024**, *57*, 103522. [[CrossRef](#)]
4. Li, Q.; Wang, C.; Liu, F.; Hu, T.; Shen, W.; Li, E.; Liao, S.; Zou, Y. Mulberry leaf polyphenols attenuated postprandial glucose absorption via inhibition of disaccharidases activity and glucose transport in Caco-2 cells. *Food Funct.* **2020**, *11*, 1835–1844. [[CrossRef](#)] [[PubMed](#)]

5. Li, Q.; Wang, Y.; Dai, Y.; Shen, W.; Zou, Y. 1-Deoxynojirimycin modulates glucose homeostasis by regulating the combination of IR-GIUT4 and ADIPO-GLUT4 pathways in 3T3-L1 adipocytes. *Mol. Biol. Rep.* **2019**, *46*, 6277–6285. [[CrossRef](#)] [[PubMed](#)]
6. Vongsak, B.; Mangmool, S.; Gritsanapan, W. Antioxidant activity and induction of mRNA expressions of antioxidant enzymes in HEK-293 Cells of Moringa oleifera leaf extract. *Planta Medica* **2015**, *81*, 1084–1089. [[CrossRef](#)]
7. Krasteva, I.; Platikanov, S.; Nikolov, S.; Kaloga, M. Flavonoids from Astragalus hamosus. *Nat. Prod. Res.* **2007**, *21*, 392–395. [[CrossRef](#)] [[PubMed](#)]
8. Li, X.; Tang, Z.; Fei, D.; Liu, Y.; Zhang, M.; Liu, S. Evaluation of the sedative and hypnotic effects of astragalin isolated from *Eucommia ulmoides* leaves in mice. *Nat. Prod. Res.* **2016**, *31*, 2072–2076. [[CrossRef](#)] [[PubMed](#)]
9. Kim, M.-S.; Kim, S.H. Inhibitory effect of astragalin on expression of lipopolysaccharide-induced inflammatory mediators through NF- $\kappa$ B in macrophages. *Arch. Pharmacol. Res.* **2011**, *34*, 2101–2107. [[CrossRef](#)] [[PubMed](#)]
10. Cho, I.H.; Gong, J.H.; Kang, M.K.; Lee, E.-J. Astragalin inhibits airway eotaxin-1 induction and epithelial apoptosis through modulating oxidative stress-responsive MAPK signaling. *BMC Pulm. Med.* **2014**, *14*, 122. [[CrossRef](#)]
11. Kim, Y.H.; Choi, Y.J.; Kang, M.K.; Park, S.H.; Antika, L.D.; Lee, E.J.; Kim, D.Y.; Kang, Y.H. Astragalin inhibits allergic inflammation and airway thickening in ovalbumin-challenged mice. *J. Agric. Food Chem.* **2017**, *65*, 836–845. [[CrossRef](#)]
12. Wei, M.; Mahady, G.B.; Liu, D.; Zheng, Z.S.; Lu, Y. Astragalin, a flavonoid from *Morus alba* (mulberry) increases endogenous estrogen and progesterone by inhibiting ovarian granulosa cell apoptosis in an aged rat model of menopause. *Molecules* **2016**, *21*, 675. [[CrossRef](#)]
13. Lordan, S.; Smyth, T.J.; Soler-Vila, A.; Stanton, C.; Ross, R.P. The  $\alpha$ -amylase and  $\alpha$ -glucosidase inhibitory effects of Irish seaweed extracts. *Food Chem.* **2013**, *141*, 2170–2176. [[CrossRef](#)]
14. Dirir, A.M.; Daou, M.; Yousef, A.F.; Yousef, L.F. A review of alpha-glucosidase inhibitors from plants as potential candidates for the treatment of type-2 diabetes. *Phytochem. Rev.* **2022**, *21*, 1049–1079. [[CrossRef](#)]
15. Zhang, B.; Zhou, G.; Li, C. AMPK: An emerging drug target for diabetes and the metabolic syndrome. *Cell Metab.* **2009**, *9*, 407–416. [[CrossRef](#)] [[PubMed](#)]
16. Liao, B.; Qin, Y.; Pan, S.; Wang, G.; Jiang, Z.; Li, B.; Wang, Y.; Wang, Y.; Zhou, M.; Zhang, Y.; et al. AICAR-based exercise mimetic alleviates aging-induced memory impairment through activating AMPK and improving mitochondrial quality control. *Food Sci. Hum. Wellness* **2024**, *15*, 9250325. [[CrossRef](#)]
17. Ozaki, Y.; Ohashi, K.; Otaka, N.; Kawanishi, H.; Takikawa, T.; Fang, L.; Takahara, K.; Tatsumi, M.; Ishihama, S.; Takefuji, M. Myonectin protects against skeletal muscle dysfunction in male mice through activation of AMPK/PGC1 $\alpha$  pathway. *Nat. Commun.* **2023**, *14*, 4675. [[CrossRef](#)] [[PubMed](#)]
18. Aggarwal, S.; Wang, Q.; Shailendra, G.; Ribnichy, D.; Burk, D.; Cefalu, W. An extract of *Artemisia dracunculus* L. stimulates insulin secretion from beta cells, activates AMPK and suppresses inflammation. *J. Ethnopharmacol.* **2015**, *170*, 98–105. [[CrossRef](#)] [[PubMed](#)]
19. Xie, L.; Zhang, T.; Karrar, E.; Zheng, L.; Xie, D.; Jin, J.; Chang, M.; Wang, X.; Jin, Q. Insights into an  $\alpha$ -Glucosidase Inhibitory Profile of 4,4-Dimethylsterols by Multispectral Techniques and Molecular Docking. *J. Agric. Food Chem.* **2021**, *69*, 15252–15260. [[CrossRef](#)] [[PubMed](#)]
20. Ferrer-Gallego, R.; Alves, R.G.; Rivas-Gonzalo, J.C.; Escribano-Bailon, M.T.; Freitas, V.D. Interaction of phenolic compounds with bovine serum albumin (BSA) and  $\alpha$ -amylase and their relationship to astringency perception. *Food Chem.* **2012**, *135*, 651–658. [[CrossRef](#)] [[PubMed](#)]
21. He, M.; Zhai, Y.; Zhang, Y.; Xu, S.; Yu, S.; Wei, Y.; Xiao, H.; Song, Y. Inhibition of  $\alpha$ -glucosidase by trilobatin and its mechanism: Kinetics, interaction mechanism and molecular docking. *Food Funct.* **2022**, *13*, 857–866. [[CrossRef](#)] [[PubMed](#)]
22. Zou, Y.; Mei, C.; Liu, F.; Xing, D.; Pang, D.; Li, Q. The lipase inhibitory effect of mulberry leaf phenolic glycosides: The structure-activity relationship and mechanism of action. *Food Chem.* **2024**, *458*, 140228. [[CrossRef](#)]
23. Li, Q.; Liu, F.; Liao, S.; Zhou, D.; Xing, D.; Zou, Y. Targeted and non-targeted metabolic characteristics of 6,7-dihydroxy-2,4-dimethoxy-phenanthrene during simulated gastrointestinal digestion. *Food Chem.* **2024**, *464*, 141534. [[CrossRef](#)] [[PubMed](#)]
24. Genheden, S.; Ryde, U. The MM/PBSA and MM/GBSA methods to estimate ligand-binding affinities. *Expert Opin. Drug Discov.* **2015**, *10*, 449–461. [[CrossRef](#)] [[PubMed](#)]
25. Cao, M.; Wang, J.; Jiang, X.; Sun, Z.; Zhao, L.; Chen, G. Phenolic constituents from Black Quinoa alleviate insulin resistance in HepG2 cells via regulating IRS1/PI3K/Akt/GLUTs signaling pathways. *J. Agric. Food Chem.* **2023**, *48*, 71. [[CrossRef](#)]
26. Li, Y.; Zhou, F.; Gao, F.; Bian, J.; Shan, F. Comparative Evaluation of Quercetin, Isoquercetin and Rutin as Inhibitors of  $\alpha$ -Glucosidase. *J. Agric. Food Chem.* **2009**, *57*, 11463–11468. [[CrossRef](#)] [[PubMed](#)]
27. Songsong, Z.; Beibei, Q.; Jinhua, Z.; Khan, M.Z.H.; Xiuhua, L. Investigation of the interaction of 2,4-dimethoxy-6,7-dihydroxyphenanthrene with  $\alpha$ -glucosidase using inhibition kinetics, CD, FT-IR and molecular docking methods. *Spectrochim. Acta Part A Mol. Biomol. Spectrosc.* **2018**, *203*, 13–18.
28. Hu, W.; Cao, G.; Zhu, J.; Li, J.; Liu, X. Naturally occurring Batatasins and their derivatives as alpha-glucosidase inhibitors. *RSC Adv.* **2015**, *5*, 82153–82158. [[CrossRef](#)]

29. Ma, R.; Weng, H.; Liang, J. Screening of lipase inhibitors in Folium Mori with lipase-linked magnetic microspheres by high-performance liquid chromatography and evaluation in diabetic mice. *J. Sep. Sci.* **2016**, *39*, 4474–4483. [[CrossRef](#)] [[PubMed](#)]
30. Ke, M.; Hu, X.Q.; Ouyang, J.; Dai, B.; Xu, Y. The effect of astragaloside on the VEGF production of cultured Müller cells under high glucose conditions. *Bio-Med. Mater. Eng.* **2012**, *22*, 113–119. [[CrossRef](#)]
31. Genovese, D.; Cingolani, M.; Rampazzo, E.; Prodi, L.; Zaccheroni, N. Static quenching upon adduct formation: A treatment without shortcuts and approximations. *Chem. Soc. Rev.* **2021**, *50*, 8414–8427. [[CrossRef](#)] [[PubMed](#)]
32. Su, H.; Ruan, Y.; Li, Y.; Chen, J.; Yin, Z.; Zhang, Q. In vitro and in vivo inhibitory activity of taxifolin on three digestive enzymes. *Int. J. Biol. Macromol.* **2020**, *150*, 31–37. [[CrossRef](#)] [[PubMed](#)]
33. Huang, Y.; Richardson, S.J.; Brennan, C.S.; Kaspas, S. Mechanistic insights into  $\alpha$ -amylase inhibition, binding affinity and structural changes upon interaction with gallic acid. *Food Hydrocoll.* **2024**, *148*, 109467. [[CrossRef](#)]
34. Zhang, J.; Sun, L.; Dong, Y.; Fang, Z.; Nisar, T.; Zhao, T.; Wang, Z.-C.; Guo, Y. Chemical compositions and  $\alpha$ -glucosidase inhibitory effects of anthocyanidins from blueberry, blackcurrant and blue honeysuckle fruits. *Food Chem.* **2019**, *299*, 125102. [[CrossRef](#)] [[PubMed](#)]
35. Zhang, G.; Hu, Y.; Pan, J. Interaction between toddalolactone and human serum albumin. *J. Solut. Chem.* **2014**, *43*, 727–745. [[CrossRef](#)]
36. Zhang, X.; Li, D.; Wang, K.; Xie, J.; Liu, Y.; Wang, T.; Liu, S.; Huang, Q.; Guo, Q.; Wang, H. Hyperoside inhibits pancreatic lipase activity in vitro and reduces fat accumulation in vivo. *Food Funct.* **2023**, *14*, 4763–4776. [[CrossRef](#)]
37. Han, L.; Chun, F.; Zhu, R.; Qiang, P.; Li, D.; Wang, M. Inhibitory effect of phloretin on  $\alpha$ -glucosidase: Kinetics, interaction mechanism and molecular docking. *Int. J. Biol. Macromol.* **2017**, *95*, 520–527. [[CrossRef](#)]
38. Ni, M.; Hu, X.; Gong, D.; Zhang, G. Inhibitory mechanism of vitexin on  $\alpha$ -glucosidase and its synergy with acarbose. *Food Hydrocoll.* **2020**, *105*, 105824. [[CrossRef](#)]
39. Yang, J.; Wang, X.; Zhang, C.; Ma, L.; Wei, T.; Zhao, Y.; Peng, X. Comparative study of inhibition mechanisms of structurally different flavonoid compounds on  $\alpha$ -glucosidase and synergistic effect with acarbose. *Food Chem.* **2021**, *347*, 129056. [[CrossRef](#)] [[PubMed](#)]
40. Hongjin, T.; Huang, L.; Chunyong, S.; Dongsheng, Z. Exploring the structure–activity relationship and interaction mechanism of flavonoids and  $\alpha$ -glucosidase based on experimental analysis and molecular docking studies. *Food Funct.* **2020**, *11*, 3332–3350.
41. Santana, D.; Trindade, I.; Carvalho, Y.; Carvalho-Neto, A.; Silva, E.; Silva-Júnior, E.; Leite, R.; Quintans-Júnior, L.; Aquino, T.; Serafini, M.; et al. Analytical techniques to recognize inclusion complexes formation involving monoterpenes and cyclodextrins: A study case with (–) borneol, a food ingredient. *Food Chem.* **2021**, *339*, 127791. [[CrossRef](#)] [[PubMed](#)]
42. Cordero-Herrera, I.; Martín, M.A.; Bravo, L.; Goya, L.; Ramos, S. Cocoa flavonoids improve insulin signalling and modulate glucose production via AKT and AMPK in HepG2 cells. *Mol. Nutr. Food Res.* **2013**, *57*, 974–985. [[CrossRef](#)]
43. Wang, Y.Y.; Chen, C.J.; Lin, S.Y.; Chuang, Y.H.; Tung, K.C. Hyperglycemia is associated with enhanced gluconeogenesis in a rat model of permanent cerebral ischemia. *Mol. Cell Endocrinol.* **2013**, *367*, 50–56. [[CrossRef](#)] [[PubMed](#)]
44. Jarinyaporn, N.; Patchareewan, P.; Veerapol, K.; Auemduan, P.; Upa, K.; Arunporn, I. Mulberry leaf extract stimulates glucose uptake and GLUT4 translocation in rat adipocytes. *Am. J. Chin. Med.* **2012**, *40*, 163–175.
45. Gao, M.; Liu, D. Resveratrol suppresses T0901317-induced hepatic fat accumulation in mice. *AAPS J.* **2013**, *15*, 744–752. [[CrossRef](#)] [[PubMed](#)]
46. Yoon, S.A.; Kang, S.I.; Shin, H.S.; Kang, S.W.; Kim, S.J. P-Coumaric acid modulates glucose and lipid metabolism via AMP-activated protein kinase in L6 skeletal muscle cells. *Biochem. Biophys. Res. Commun.* **2013**, *432*, 553–557. [[CrossRef](#)]
47. Zhang, Y.; Huang, Z.; Han, W.; Wu, J.; Li, S.; Qin, T.; Zhang, C.; Shi, M.; Han, S.; Gao, B. Glutamine suppresses senescence and promotes autophagy through glycolysis inhibition-mediated AMPK $\alpha$  lactylation in intervertebral disc degeneration. *Commun. Biol.* **2024**, *7*, 325. [[CrossRef](#)] [[PubMed](#)]
48. Li, J.; Yin, M.; Wang, Z.; Xiong, Y.; Fang, X.; Fang, H. Fingolimod alleviates type 2 diabetes associated cognitive decline by regulating autophagy and neuronal apoptosis via AMPK/mTOR pathway. *Brain Res.* **2025**, *1846*, 149241. [[CrossRef](#)] [[PubMed](#)]

**Disclaimer/Publisher’s Note:** The statements, opinions and data contained in all publications are solely those of the individual author(s) and contributor(s) and not of MDPI and/or the editor(s). MDPI and/or the editor(s) disclaim responsibility for any injury to people or property resulting from any ideas, methods, instructions or products referred to in the content.